

Title: Target Selection Method in Atlas Construction based on Multidimensional Scaling

Authors: Hyunjin Park, Peyton H. Bland, Alfred O. Hero III, and Charles R. Meyer

Abstract: Probabilistic atlases provide pivotal information for medical image segmentation and registration. Typically an atlas has been built on a common target image space which other training images are mapped onto. This introduces bias towards to the chosen target. Here we present a method to choose a target image which has the least bias considering all training images. Our method chooses a target image that is the closest to the mean geometry of the training images determined by bending energy. Our approach is based on forming a distance matrix based on bending energies of all pair-wise registrations and performing multidimensional scaling (MDS) on the distance matrix.

Keywords: Atlas Construction, Target Selection, Multidimensional Scaling.

Send all correspondence to:

Charles R. Meyer

Department of Radiology, #3307 Kresge III

University of Michigan, Ann Arbor, MI 48109, U.S.A.

cmeyer@umich.edu

Office: 1-734-763-5881 Fax: 1-734-764-8541

<http://www.dipl.rad.med.umich.edu/>

Supported in part by the U.S. National Institute of Health under grant 1P01CA87684.

1. Introduction

As more medical images are collected on a routine basis, study of images of multiple patients or a population becomes feasible. The study of images of a population leads to statistics of the population, which manifests itself in a probabilistic atlas. Probabilistic atlases have been very useful to bring prior information to medical image segmentation and registration especially for brain [1, 17]. Segmentation algorithms use atlas information as prior probability in Bayesian framework or as a starting guess [2]. Atlas information guides segmentation algorithms where there is little grayscale information available. For example atlas information may be able to differentiate between body wall and liver where the grayscale information in a non-contrast CT is almost identical. Registration algorithms can benefit from the atlas information as a prior on a distribution of a displacement field [3].

Typically researchers first build their atlas by picking a target image and mapping other training images onto the target image. Statistical processing can be performed on the same spatial frame after all images are mapped onto the target image. Statistical processing can be as simple as a simple grayscale average or some measure of probability at every voxel location. Methods for registration (i.e., mapping) in terms of degrees of freedom (DOF) and geometric interpolant have to be the same for all registration tasks to ensure consistent construction and use of the atlas. The resulting atlas is inherently biased by the choice of the chosen target image. The atlas does not represent the population effectively if the target image is an extreme of the population. Applying the atlas to a test image involves registering the test image with the atlas. This task of bringing in the atlas information to the test image becomes difficult if the atlas is built on an extreme case of the population. In this case, the geometric distance the test image has to travel to reach the atlas has been increased compared to the case of reaching an atlas which resides at the mean geometry of the population. The bias towards a specific target may be reduced if the whole process of mapping other images onto the target is repeated with the target replaced with an average image from the previous registrations until the average image converges [4].

Studholme et al. proposed a method to jointly register all images simultaneously to a target space that is very close to the mean geometry [5]. In this approach, there is very little bias since the target image space is very close to the mean geometry. They register all images at the same time using a cost function that encourages mean displacement field from the target

onto other images to be an identity transform and minimizes the joint entropy of all images. All displacement fields to other images have to be known to compute the mean displacement field. Thus their approach, which requires registration of all images simultaneously, increases the dimensionality of the optimization space tremendously.

Joshi et al. proposed an atlas construction independent of choosing a specific target image [6]. First an arbitrary image is chosen as a target and the rest of the training images are mapped onto the target. Once the mappings are finished an atlas is created on the target image space. After the atlas is constructed on the target image space, the atlas is warped onto a space where there is less bias towards the rest of the images. The warping involved is derived from the mean displacement field. In theory, they can choose any target image and arrive at the same atlas space since the atlas calculated on a specific target image space is always going to be warped onto another space where there is less bias. Their method has certain limitations, which will be discussed in the discussion section (i.e., section 5).

Marsland et al. proposed to construct an atlas on a target image that is close to the mean geometry of the training images [7]. They choose the target image such that the sum of distances from the target image to the rest of the images is minimized. Our method of target selection in this paper shares a similar approach. Improvements in our approach will be shown in the discussion section.

The above is a brief overview of existing methods of atlas construction. Details of the existing methods and comparison with our approach will be given in the discussion section. We present an alternative approach to unbiased atlas construction methods robust to effects of imperfect registrations. Here we present a method to choose a target image that is the closest to the mean geometry of the population. Our approach is based on forming a distance matrix based on bending energies of all pair-wise registrations and performing multidimensional scaling (MDS) on the distance matrix to find the best target. The paper is organized as the following. Section 2 includes an overview of the method of target selection, section 3 includes a validation of the method on simulated 2D cases, section 4 contains an application of the method to 3D scans, and sections 5 and 6 contain the discussion and summary of our method respectively.

2. Methods

Throughout the paper we choose the traditional approach of atlas construction, mapping other images onto a chosen target image and processing the mapped images on the target image space. Our contribution is how to choose a target image that is the least biased towards the rest of the training images.

2.1. Pair-wise Registration

Atlas construction involves many tasks of mapping one image onto another image. This task of mapping is called registration. Registration has been well reviewed in Hill's paper [8]. Basically two main components need to be addressed for any registration algorithm: the similarity measure which measures degree of alignment and the geometric interpolant which defines the geometric transform between two images. We choose mutual information (MI) as the similarity measure and thin-plate splines (TPS) as the geometric interpolant [9]. Mutual information between image A and B is defined as below,

$$MI(A, B) = \sum \sum p(a, b) \log_2 \left(\frac{p(a, b)}{p(a)p(b)} \right) \quad (1)$$

$p(a), p(b)$; marginal density of image A and B

$p(a, b)$; joint density of image A and B.

A simple histogram with fixed bin width is used to calculate the probability density function of grayscale value distributions. Thin-plate splines in 2D is defined as below,

$$f_x(x, y) = a_0 + a_1x + a_2y + \sum_{i=1}^N w_i r^2 \log(r^2) \quad (2)$$

$$r^2 = (x - x_i)^2 + (y - y_i)^2$$

a_0, a_1, a_2 ; affine parameters w_i ; warp coefficient

$f_x(x, y)$; displacement in x (x_i, y_i) ; control point locations

N; number of control points.

In similar fashion to (2) displacement in y direction can be defined as well. Thin-plate splines in 3D is also defined in a similar fashion except that the basis function is replaced with $|r|$. The process of registration can be formulated as maximizing the chosen similarity measure (i.e., MI) under a hypothetical geometric transform,

$$\hat{T} = \arg \max_{T \in F} MI(A(\bullet), B(T(\bullet))) \quad (3)$$

\hat{T} ; estimate of the transform

F ; family of feasible transforms.

A simplex optimizer is used to maximize the cost function [9].

2.2. Distance Measure

The outcome of image registration is a geometric transform optimized to maximize a certain cost function (e.g., MI). The displacement field is computed by evaluating the geometric transform at every pixel location. The geometric distance, hereafter called distance, between two images is often measured by the roughness of the geometric transform that associates coordinate spaces of two images. We design the distance to have invariance to affine transforms. For example, if two images can be registered perfectly with an affine transform, then it implies that two images are essentially composed of the same objects but lying in different coordinate spaces, thus a value of zero is assigned to the distance. Roughness of the geometric transform can be measured by integrating squared value of n-th order partial derivatives of the transform. Second order derivatives are chosen to ensure invariance to affine transforms. We define the distance between two images as the sum of squared second order partial derivatives of the geometric transform,

$$d^2 = \iint \left(\frac{\partial^2 f_x}{\partial x^2} \right)^2 + 2 \left(\frac{\partial^2 f_x}{\partial x \partial y} \right)^2 + \left(\frac{\partial^2 f_x}{\partial y^2} \right)^2 dx dy + \quad (4)$$

$$\iint \left(\frac{\partial^2 f_y}{\partial x^2} \right)^2 + 2 \left(\frac{\partial^2 f_y}{\partial x \partial y} \right)^2 + \left(\frac{\partial^2 f_y}{\partial y^2} \right)^2 dx dy$$

f_x ; displacement in x f_y ; displacement in y.

The above formulation is for 2D and can be easily extended for 3D. This distance is often called the bending energy. An analytic formula for calculating bending energy is available for TPS [10]. For other geometric transforms, the bending energy may need to be calculated numerically. The bending energy of TPS is the smallest for all interpolating splines and has the property of removing affine differences in the transform. The defined distance in (4) is not a metric since the distance between two different images can be zero if two images are registered by an affine transform. A metric distance yields zero when the objects (e.g.,

images) of comparison are identical. There are two more properties that a metric should satisfy: symmetry and triangular inequality. If the requirement of invariance to affine transform is dropped, others have proposed a distance satisfying all three properties of metric [11, 12]. In those cases the distance is defined as a Sobolev norm on the displacement field or the velocity field. One example of a metric distance is the viscous fluid model where the distance is invariant to only an identity transform [13]. We choose our distance to have invariance to affine transform at the expense of not satisfying the property of a metric. Devising a metric distance is left for future work. Symmetry of the distance is not guaranteed but the distance matrix can be rendered symmetric as will be discussed in section 2.6 and 3.6.

2.3. Multidimensional Scaling (MDS)

Multidimensional scaling (MDS) is a technique to produce relative positional locations in a space of dimension d from a collection of pair-wise distances [14, 15]. For example, given pair-wise Euclidean distances between North American cities, two dimensional MDS will yield a map of relative locations of those cities. The relative locations are accurate up to arbitrary rotate-translate transform. For N cities, $N(N-1)/2$ (i.e., N choose 2) pair-wise distances are needed. The distances used in MDS need not be metric, as non-metric distances (e.g., ranking) can be used. Thus, our distance defined in section 2.2 can be used in MDS settings. MDS has its roots in psychometrics but has been widely used in other fields as a tool to gain insight to data relationships. Given a set of distances in the distance matrix D , where an element of matrix d_{ij} refers to the distance between objects i and j , MDS outputs a set of coordinates in a user specified dimension that reproduces the distance matrix best in the least square fashion. The dimension of MDS output, called the embedding dimension, may be estimated by either thresholding the scree plot of eigenvalues of the distance matrix or by more direct approaches such as the manifold learning based on entropic graphs [20]. More details on the entropic graph based manifold learning will be covered in section 3.3. The output coordinates are in the standard Euclidean space of the user chosen dimension. The diagonal elements of the distance matrix are zero by definition. The number of dimensions is user controllable and should be determined to be the smallest number that allows meaningful description of all the pair-wise distances.

2.4. Target selection based on MDS

An ideal target image is the one that resides at the mean geometry of the population in atlas construction. The sum of distances to other images from the atlas space (i.e., target space) is minimized for the ideal target image. For a target image space that is far away from the mean geometry, the sum of distances to other images will be greater. Often there may not be an image at the mean geometry; thus the best approach in picking a target image, which yields the minimum distance to other images, is to choose the image that is the closest to the mean geometry. The described approach works only if we know all the relative locations of images of the population so that the location for the mean geometry can be calculated. MDS identifies all the relative locations of the images from the distance matrix. The elements of the distance matrix are determined by the distances of pair-wise registrations. In summary, we select the target image which is the closest to the mean geometry with the aid of information of relative locations provided by MDS. MDS in turn requires a distance matrix whose elements are calculated from pair-wise registrations. The following is the procedure for N images,

1. Perform $N(N-1)/2$ pair-wise registrations
2. Calculate bending energies from the registrations
3. Form distance matrix D
4. Determine embedding dimension of MDS
5. Apply MDS and find relative locations of images
6. Calculate mean location of the images
7. Choose target image that is the closest to the mean.

Once the best (i.e., the closest to the mean geometry) target is selected, all other images can be mapped onto the chosen target with ease, this step is trivial since all pair-wise registrations have been computed previously to fill the distance matrix.

2.5. Robustness to Mis-registration

The result of pair-wise registration is characterized by the geometric transform or the displacement field between two images. In the MDS framework, we compress the whole displacement field, whose DOF are on the order of the number of pixels, to a single scalar value noted as distance. The effects of imperfect registrations will be less evident on the single scalar value than the whole displacement field. But if we stop here we lose the

sensitivity of the displacement field to shape change by compressing it to a single scalar. In addition, we make multiple measurements of the single scalar value (i.e., distance) between various configurations to improve the sensitivity to shape change. For example, for N scans, instead of computing $N-1$ displacement fields and distances with respect to a chosen target image, we compute displacement fields and distances with respect to all possible pairs of target and source images, i.e. N choose 2 = $N(N-1)/2$ images. Multiple distance measurements correspond to pair-wise distances in MDS framework. Robustness of MDS framework regarding mis-registrations will be shown for simulated 2D images in section 3.4.

2.6. Distance Matrix

A distance matrix is required for MDS as an input. The distance matrix can be either symmetric or asymmetric. For a symmetric distance matrix (i.e., $d_{ij} = d_{ji}$), distance between object i and j is order independent. In atlas construction, it implies that the distance between image i as the reference image and image j as the floating image is the same as the distance between images i and j switching the role of the reference and the floating image. In practice, switching the order of images in the registration may yield a different geometric transform thus it may yield a different distance value with TPS based registrations, but the discrepancy in distance values is quite small provided that the DOF of TPS is high enough. Even for an asymmetric distance matrix (i.e., $d_{ij} \neq d_{ji}$), the distance matrix can be made symmetric by using the average value of d_{ij} and d_{ji} . For computational savings, we assume a symmetric distance matrix thus only the upper half of the distance matrix is computed and the lower half of the matrix is replicated. Employing an asymmetric distance matrix will require twice the number of pair-wise registrations (i.e., $N(N-1)$) since all elements except for the diagonal elements need to be calculated. While the computation burden increases for an asymmetric distance matrix, it will be more tolerant to errors in the distance matrix as in the case of low DOF registration where there is a possibility of substantial discrepancy between d_{ij} and d_{ji} . Effects of using an asymmetric distance matrix will be discussed for 2D simulated cases in section 3.6.

3. 2D Synthetic Experiments

Synthetic experiments are carried out in 2D to show the feasibility of our approach of target selection.

3.1. Experiment Setup

A synthetic MRI slice from BRAINWEB simulation is obtained [16]. The slice has 256×256 dimension and $1 \times 1 \text{ mm}^2$ resolution. It is deformed in a known way using $6 \times 6 = 36$ knots of B-splines resulting in 50 deformed images. Deformations are applied by randomly choosing a knot and displacing the knot by the amount determined by zero mean Gaussian of variance 100 pixels in both x and y direction. After the image's geometry is deformed, a zero mean Gaussian noise of variance 16 is added to the image's grayscale values. One sample deformation is described in Figure 1. Six images of the known 50 deformed images are shown in Figure 2. The atlas is constructed with these 50 deformed images. Geometric distances from the original undeformed image (i.e., BRAINWEB image) to all 50 images are calculated given all the known synthetic deformations and are shown in Table 1. We verified that the mean displacement field from the original image to other deformed images is very close to an identity transform (i.e., root mean squared error with respect to the identity transform is less than 0.1 pixel). The best possible target image is the closest image to the original image since the original image is absent from the 50 training images. Ground truth on what is the best target image can be established based on the distances from the original image. In addition, the quality of all potential target images can be rank ordered according to the distances from the original image.

3.2. Results

Pair-wise registrations of the 50 images are performed using 25 uniformly distributed control points as described in Figure 3. There are 1225 (i.e., 50 choose 2) pair-wise registrations required to fill up the symmetric 50×50 distance matrix; only the upper half of the distance matrix is filled and the lower half is duplicated. After the distance matrix is computed, MDS is performed with 4 dimensions. The dimension is determined by the entropic graph based manifold learning. More details on how to choose the dimension appear in the next section. The output of the MDS is 50 coordinates in 4 dimensions representing the 50 images in the Euclidean space. Two dimensional projections (out of

total of 4) of these coordinates are shown in Figure 4. The location of the mean geometry of the 50 images is calculated by taking an arithmetic mean of 50 coordinates, which is set to be the origin (i.e., $(0,0,0,0)$). The image whose coordinate is the closest to the mean geometry is chosen to be the best target image. Distances from the mean geometry (i.e., origin) to the images (i.e., MDS coordinates) are sorted in Table 2 starting from the closest image to the furthest image. The best target image from the MDS output (i.e., the first image in Table 2) is image 2, which coincides with the best target from the ground truth (i.e., the first image in Table 1). Thus our selected target is the closest image from the mean geometry. Moreover comparison of the ordering of images in Table 1 and 2 indicates that MDS results in Table 2 are very similar to the ground truth in Table 1. We are able to replicate the order of images reasonably well from MDS results, not just the closest image to the mean geometry. In fact, the root mean squared error, defined as the root mean squared value of the difference in the rank order of images between Table 1 and 2, is computed to be 0.3980. Hereafter we note the error as rank order error.

3.3. Determining the embedding dimension for MDS

An essential step in implementing MDS is the determination of an appropriate embedding dimension d for positioning the N points described by the pairwise distance matrix. When the set of points is known to lie on a hyperplane of known dimension, the embedding dimension should be selected as equal to this dimension. For example in geographic location problems, e.g., in [18], the choice of embedding dimension $d = 2$ is obvious. In other cases the points may not lie in any natural or physical domain and the points can only be assumed to vary over some space having dimension less than N . A standard way of estimating this dimension is to perform a sequence of MDS projections, successively increasing the dimension at each iterate, and detecting a knee in the set of fitting errors, defined as the Frobenius norm of the difference between the distance matrix of the projected sample and the original distance matrix. This is equivalent to choosing the embedding dimension by thresholding the scree plot of ordered eigenvalues of the centered distance matrix. A major issue in scree plot thresholding methods is the suitable choice of threshold.

Recently a class of statistically sound dimension estimation methods based on manifold learning have been proposed that are more reliable than ad hoc scree plot thresholding.

These methods directly estimate the embedding dimension from the pairwise distance matrix without the need for thresholding. The entropic graph method of Costa and Hero [20], which we adopt in this paper, extracts a statistically consistent estimate of dimension by determining the rate of growth of a sequence of k -nearest-neighbor graphs constructed from the distance matrix. The method of [20] uses bootstrap resampling to estimate a histogram of probable dimensions that are consistent with the data and the dimension estimate can then be computed as the median, mean or mode of the histogram. For the atlas construction problem of interest the dimension is extracted from the distance matrix constructed from bending energies resulting in a dimension histogram shown in Figure 5 for the experiment described in Section 3.1. The range of probable dimensions is $d=3$ to $d=6$, which is consistent with the dip in eigenvalues around dimension observed in the scree plot shown in Figure 5. The mode of the dimension histogram is equal to 4, which can be interpreted as the most probable dimension, and this was adopted as the embedding dimension for the MDS results described in section 3.2. Note that, the dimension histogram reflects the probable dimension of the actual embedding space of the points, which may in fact be a non-linear subspace. On the other hand, MDS projects onto a linear subspace so dimension estimation using the histogram mode may slightly underestimate the dimension required by the MDS algorithm. However, when we redid the analysis with slightly increased MDS dimension ($d=5$) we did not observe significantly different results than shown in section 3.2.

3.4. Robustness to Registration Error

In this section, we provide 2D simulation results regarding robustness of our MDS based approach. As indicated in section 2.5, we compress the whole displacement field to a single scalar value. In result, registration error (i.e., error in the displacement field) has less effect on the measured scalar distance value. We have performed two simulated trials. In the first trial, we add registration noise to one of the many pair-wise registrations and observe the rank order error. The rank order errors are measured as we increase the magnitude of the added registration noise to one chosen pair-wise registration. Registration noise is implemented by randomly perturbing the optimized TPS control points location by a zero mean Gaussian of appropriate standard deviation. For the first trial, we can see that the rank order error does not change much as we increase the magnitude (i.e., standard deviation) of the added registration noise as in Figure 6. The affected pair-wise registration

is between image 9 and 45. The rank order error changes little even at the standard deviation of 50 pixels where the size of the image is 256x256 pixels. In fact the rank order error stays the same value after standard deviation of 10 pixels. It implies that one erroneous pair-wise registration out of 1250 possible registrations will not affect the rank order error. As long as only one pair-wise registration is affected, we have witnessed a similar trend, relative constant rank order error with respect to increase in registration noise. In the second trial, we fix the amount of registration noise added but increase the number of pair-wise registrations affected. Zero mean Gaussian noise of standard deviation 15 pixels is added to optimized locations of TPS control points for randomly chosen pair-wise registrations. The rank order errors are measured as the number of affected pair-wise registration increases. The rank order error stays relative same but eventually increases as more pair-wise registrations are affected as in Figure 6. The rank order error with 100 (out of 1250 possible registrations, effectively 8% of 1250) erroneous registrations is fairly close to the rank order error with no affected pair-wise registrations. It implies that our MDS based approach is robust enough withstand many erroneous registrations. The robustness of the MDS based approach is partly due to the fact that limited number of dimensions is used to represent the whole distance matrix, thus limiting the effect of noise to few dimensions.

3.5. Alternatives to MDS

There are simpler ways to choose a target image based on the distance matrix than our MDS based approach but they have degraded accuracy. One can choose the image whose average distance to all other images is minimum, which is finding the “L1 median” formulated in equation 5. In this case, column wise sum of the distance matrix is sorted ascendingly to find the best target. One can also choose the image whose maximal distance to all other images is minimum, which is finding the “Minimax median” formulated in equation 5 as well. In this case, column wise maximum value of the distance matrix is sorted ascendingly to find the best target.

$$i_{best} = \arg \min_j \sum_{k \neq j} d(j, k); \text{ L1 median} \quad (5)$$

$$i_{best} = \arg \min_j \text{MAX}_{k \neq j} d(j, k); \text{ Minimax median}$$

$d(j, k)$; distance between image j and k

Both approaches find a target based on a subset of available information, instead of using

the full distance matrix as in MDS based approach, either column wise sum or column wise maximum of the distance matrix is used. The rank order errors with respect to the ground truth in Table 1 for both approaches are 0.4436 and 1.4424 respectively, larger than the error of MDS based approach of 0.3980.

3.6. Asymmetry in Distance Matrix

The effects of employing an asymmetric distance matrix are explored in this section. Here the lower half of the distance matrix is computed from additional pair-wise registrations, not duplicated from the upper half of the distance matrix. Thus, $N(N-1)$ pair-wise registrations are computed in total resulting in 2 fold increase in computation burden. The root mean squared error of differences between lower elements and upper elements of the distance matrix is 0.0041 where individual values of the matrix elements range from 0 to 0.056. The small difference between the upper and lower elements of the matrix shows that the distance matrix is fairly symmetric in the simulated case using 25 control points. As noted in section 2.5, using an asymmetric distance matrix increases the computation burden by a factor of 2, but is potentially more tolerant to inaccuracies in the distance matrix.

3.7. Additional 2D Results

One more set of synthetic experiments is performed. It has similar 50 deformed images from the BRAINWEB slice except that all B-spline knots are perturbed instead of one knot at a time. The image's geometry is deformed by displacing all B-spline knots by a zero mean Gaussian of variance 9 in both x and y directions and a zero mean Gaussian noise of variance 16 is added to the image values. Similar to the first experiment, ground truth is established by calculating the distance to the original undeformed image. After finishing all pair-wise registrations, the entropic graph dimension estimation method yielded a dimension histogram with mode at $d=5$. Performing MDS with 5 dimensions, the error in the rank ordering of the images as compared to that of the ground truth was calculated to be 0.9282. Using simpler target selection methods based on L1 median or Minimax median leads rank order errors to be 0.9411 and 2.2493 respectively. We have repeated our target selection method on a different set of 50 images and have found that our approach is still applicable.

4. 3D Experiments

We have applied our target selection method to 10 3D non-contrast abdominal CT scans. All scans contain liver, kidneys, and spinal cord. A typical scan has dimension $512 \times 512 \times 35$ and resolution $0.7 \times 0.7 \times 5$ mm³. Here we focus on constructing the atlas of the liver not all abdominal organs.

4.1. Experiment Setup

Pair-wise registrations of 10 scans are performed with 24 control points primarily located in the liver. The 24 control points are placed at approximately the same locations for all 10 scans to ensure consistency in the registration process. In addition, we mask out the scans so that the scans only contain liver and its immediate vicinity. This is to ensure that the pair-wise registrations are only driven by the liver and nothing else. An asymmetric distance matrix is used for MDS. Thus, there are 90 (= 10×9) pair-wise registrations to fill up the distance matrix. Once the distance matrix is computed, MDS is computed with 2 dimensions chosen by the entropic graph dimensionality estimation procedures described in section 3.3. From the MDS coordinates, the scan that is the closest from the mean geometry is chosen to construct an atlas. Note there is no ground truth as to what is the best target since these scans are not simulated.

4.2. Results

Manual segmentations of liver are performed by an expert and are available for all 10 scans. It is possible to map one scan onto another scan from 90 pair-wise registrations. For every scan, an atlas is built by mapping other segmented scans onto the segmented chosen target scan and computing the percentage a voxel belongs to liver. Atlas value ranges from 0 to 1, where 1 indicates the voxel always belongs to liver and 0 indicates the voxel always belongs to something other than liver for 10 segmented cases. Entropy of the atlas is computed to quantify the variability of the atlas. First, atlas values are binned to a fixed width histogram and then Shannon entropy of the normalized histogram is computed. If an atlas has a sharp spatial transition from liver to non-liver (i.e., 1 to 0), it will have low entropy values, since all voxel values tend to be concentrated around 1 and 0. For a more diffusely valued atlas, where the spatial transition occurs over larger region, there are more voxels with intermediate values, and thus the entropy of the atlas increases. A total of 10

atlases are constructed depending on the chosen target scan. Entropy values of constructed atlases range from 1.34 to 2.33. MDS results suggest that scan 4 is the closest scan from the mean geometry and the entropy of the atlas constructed using scan 4 as the target is 1.35. The best atlas (i.e., atlas with the least variability thus the smallest entropy value) is the atlas constructed on scan 8 with the entropy value 1.34. Scan 4 with entropy value 1.35 is the second best atlas, but the difference in entropy value is quite small between scan 4 and 8. MDS results also suggest that scan 3 is the furthest scan and the entropy of the atlas constructed on scan 3 is 2.33 (i.e., the largest entropy value and thus the worst atlas). Thus, MDS results can reasonably predict what target scan is the best or worst from 10 scans when constructing an atlas.

5. Discussion

Our target selection method based on MDS enables us to choose a target that is very close to the mean geometry. In addition we can locate where all images are relative to the mean geometry. Our approach is independent of the choice of the pair-wise registration method. The user can choose any reasonable combination of similarity measure and geometric interpolant, not just MI and Thin-plate splines. Our approach is also reasonably robust to imperfect pair-wise registrations.

5.1. Computation of MDS

The computational complexity of MDS is on the order of N^3 , where N is the number of objects (i.e., images). When computed on a computer cluster (e.g., a grid system), this might be significantly reduced by applying a distributed weighted modification of MDS [18]. The computational complexity of the dimension estimator [20] is $N \log N$.

5.2. Comparison with Other Methods

Studholme et al. proposed to jointly register all images simultaneously to a target space that is very close to the mean geometry [5]. They register all images simultaneously while penalizing a non-identity mean displacement field from the target onto other images and minimizing the joint entropy of all images. High dimensional probability density function needs to be estimated to calculate the joint entropy. They proposed an adhoc clustering approach where only certain areas of the high dimensional histogram are allowed to have counts. Such an adhoc approach might have problems dealing with mis-registered states

during the optimization when clusters can form virtually anywhere in the histogram and thus possibly not be counted. There is inherent difficulty to estimate entropic measures (e.g., MI) of high dimensional probability density functions using conventional methods. Hero et al. proposed a method to estimate entropic measures of high dimensional probability density functions based on the length of minimum spanning tree [19].

Joshi's approach requires only $N-1$ pair-wise registrations for N images and is independent of choosing a target image [6]. It maps all other images to the chosen target image and then calculates a mean displacement field in the target image space. If the mean displacement field is not an identity transform then it warps the atlas created on the target image space to another space using the mean displacement field. The underlying assumption is that at the mean geometry the mean displacement field with respect to other images should be an identity transform. There are certain limitations on their approach. It assumes that the geometric transform has certain "small deformation" properties; the transform, $h(x) = x + u(x)$, is close enough to an identity transform such that the composition of the transform can be approximated by the addition of two displacement fields, $h_1 \circ h_2(x) \simeq x + u_1(x) + u_2(x)$. It is also sensitive to pair-wise registration results requiring displacement fields, the optimized geometric transforms of pair-wise registrations, to be totally accurate. Any error in the registration (i.e., change in the displacement field) will affect the mean displacement field therefore will affect the final space that the atlas resides. If the chosen target image is an extreme of the population, pair-wise registrations between the target and other training images become unreliable. Thus for practical purpose, it is important to pick a target that is close to the mean geometry even for Joshi's approach so that pair-wise registrations are reliable. They also have an atlas building method where the constraint of the geometric transform is lifted so that "large scale" deformation can be accommodated [6].

Our approach and Marsland's approach share a common theme; find a target image that is the closest to the mean geometry [7]. Their method tries to minimize not only the sum of distances to all other image but also the sum of similarity measure between the target and other images. In their algorithm, they start with an initial guess of the target image and try to update the target image if the sum of distances decreases and the sum of MI increases. We believe target should be chosen solely on distances to arrive as closely as possible to the

mean geometry. For example, if the ideal target image at the mean geometry happens to be noisy, under Marsland's approach it will never be selected as the target since choosing the ideal target will surely decrease the sum of MI. Their method is tied to a specific geometric interpolant, clamped-plate spline, while our approach can be applied to any geometric interpolant.

6. Summary

We have shown a method to choose a target image that is very close to the mean geometry. It is based on information of relative locations provided by MDS. MDS requires a distance matrix whose elements are calculated from pair-wise registrations.

Acknowledgements

The authors sincerely thank Kevin Carter for the work regarding the entropic graph based dimension estimation procedure.

References

- [1] M. B. Cuadra, C. Pollo, A. Bardera, O. Cuisenaire, J.-G. Villemure, and J.-P. Thiran, "Atlas-based segmentation of pathological MR brain images using a model of lesion growth," *IEEE Transactions on Medical Imaging*, vol. 23, pp. 1301-1314, 2004.
- [2] H. Park, P. H. Bland, and C. R. Meyer, "Construction of an abdominal probabilistic atlas and its application in segmentation," *IEEE Transaction on Medical Imaging*, vol. 22, pp. 483-492, 2003.
- [3] P. M. Thompson and A. W. Toga, "Detection, visualization and animation of abnormal anatomic structure with a deformable probabilistic brain atlas based on random vector field transformations," *Medical Image Analysis*, vol. 1, pp. 271-294, 1997.
- [4] A. W. Toga and P. M. Thompson, "The role of image registration in brain mapping," *Image and Vision Computing*, vol. 19, pp. 3-24, 2001.
- [5] C. Studholme and V. Cardenas, "A template free approach to volumetric spatial normalization of brain anatomy," *Pattern Recognition Letters*, vol. 25, pp. 1191-1202, 2004.
- [6] S. Joshi, B. Davis, M. Jomier, and G. Gerig, "Unbiased diffeomorphic atlas construction for computational anatomy," *NueroImage*, vol. 23, pp. s151-s160, 2004.
- [7] S. Marsland, C. J. Twining, and C. J. Taylor, "Groupwise non-rigid registration using polyharmonic clamped-plate splines," *Lecture Notes in Computer Science*, vol. 2879, pp. 771-779, 2003.
- [8] D. L. G. Hill, P. G. Batchelor, M. Holden, and D. J. Hawkes, "Medical image registration," *Physics in medicine and biology*, vol. 46, pp. r1-r45, 2001.
- [9] C. Meyer, J. Boes, P. Bland, K. Zasandy, P. Kison, K. Koral, K. Frey, and R. Wahl, "Demonstration of accuracy and clinical versatility of mutual information for automatic multimodality image fusion using affine and thin plate spline warped geometric deformations," *Medical Image Analysis*, vol. 3, pp. 195-206, 1997.
- [10] F. L. Bookstein, "Principal warps: thin-plate splines and the decomposition of deformations," *IEEE trans. on pattern analysis and machine intelligence*, vol. 11, pp. 567-585, 1989.
- [11] M. I. Miller and L. Younes, "Group actions, homeomorphism, and mapping: a general framework," *International Journal of Computer Vision*, vol. 41, pp. 61-84, 2001.
- [12] M. I. Miller, A. Trouve, and L. Younes, "On the metrics and euler-lagrange equations of computational anatomy," *Annuual Review of Biomedical Engineering*, vol. 4, pp. 375-405, 2002.

- [13] G. E. Christensen, R. D. Rabbitt, and M. I. Miller, "Deformable templates using large deformation kinetics," *IEEE Transactions on Image Processing*, vol. 5, pp. 1435-1447, 1996.
- [14] W. S. Torgerson, "Multidimensional scaling: I. Theory and method," *Psychometrika*, vol. 17, pp. 401-409, 1952.
- [15] F. W. Young and R. M. Hamer, *Theory and application of Multidimensional scaling*: Eribaum Associates, 1994.
- [16] D. L. Collins, A. P. Zijdenbos, A. P. Kollokian, J. G. Sled, N. J. Kabani, C. J. Holmes, and A. C. Evans, "Design and Construction of a Realistic Digital Brain Phantom," *IEEE Transaction on Medical Imaging*, vol. 17, pp. 463-468, 1998.
- [17] A. C. Cocosco, A. P. Zijdenbos, and A. C. Evans, "Automatic Generation of Training Data for Brain Tissue Classification from MRI," *Lecture Notes in Computer Science*, vol. 2488, pp. 516-523, 2002.
- [18] J. A. Costa, N. Patwari, and A. O. Hero, "Distributed Multidimensional Scaling with Adaptive Weighting for Node Localization in Sensor Networks," *to appear in ACM Transactions on Sensor Networks*, 2005.
- [19] A. O. Hero, B. Ma, O. Michel, and J. Gorman, "Application of entropic spanning graphs," *IEEE Signal Processing Magazine*, vol. 19, pp. 85-95, 2002.
- [20] J. A. Costa and A. O. Hero, "Geodesic Entropic Graphs for Dimension and Entropy Estimation in Manifold Learning," *IEEE Transactions on Signal Processing*, vol. 52, pp. 2210-2221, 2004.

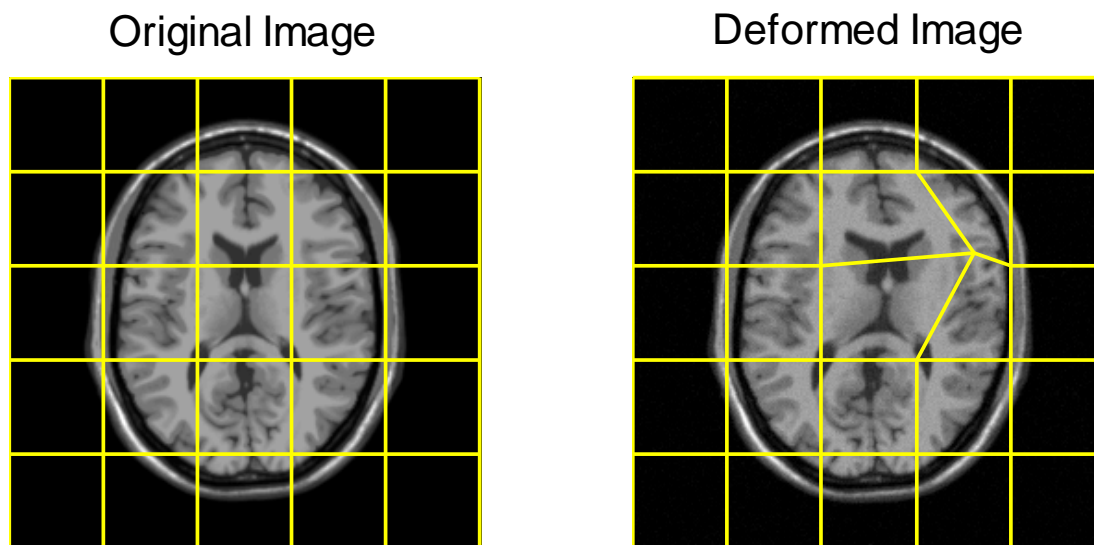


Fig. 1. Synthetic image deformation. The left figure is the original image and the right figure is the deformed image by a 6x6 B-spline deformation and added Gaussian image noise of variance 16. Grid lines show the applied B-spline deformations. Fifty deformed images are formed similarly.

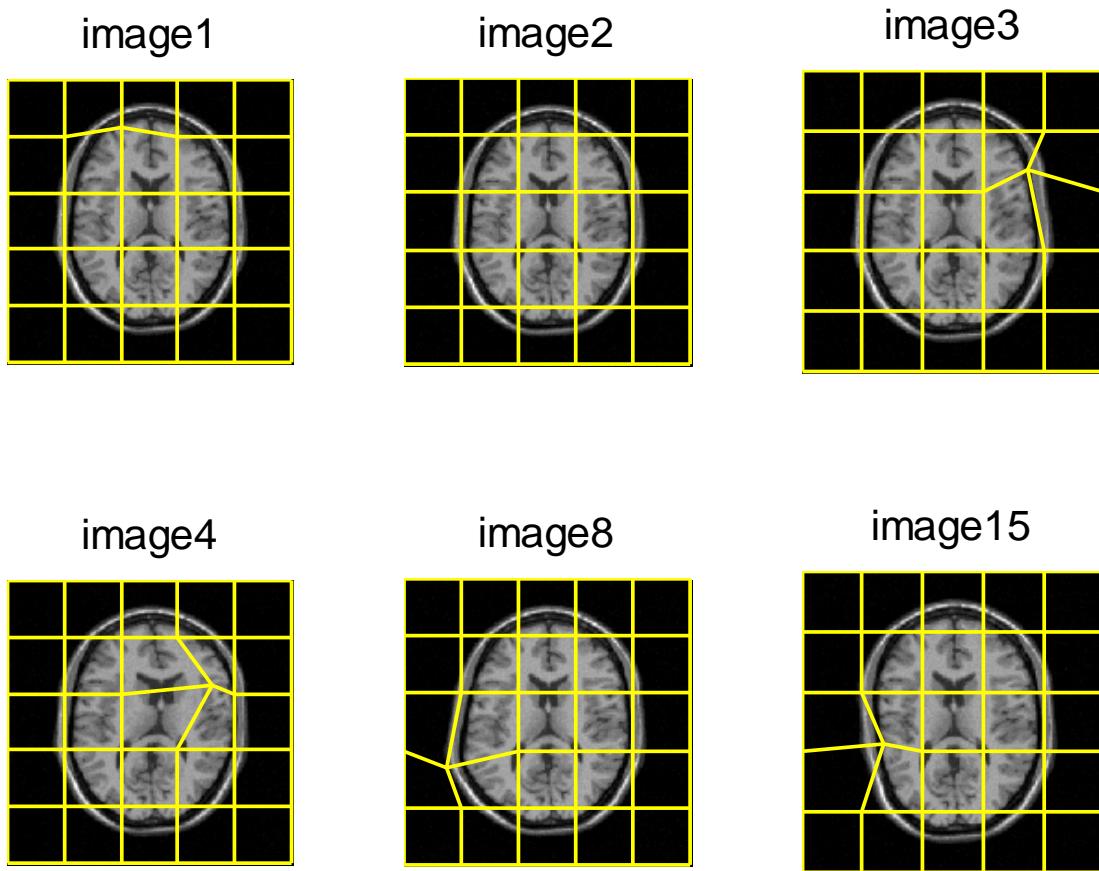


Fig. 2. Six images of the known 50 deformed images. Grid lines show the applied B-spline deformations.

Original image

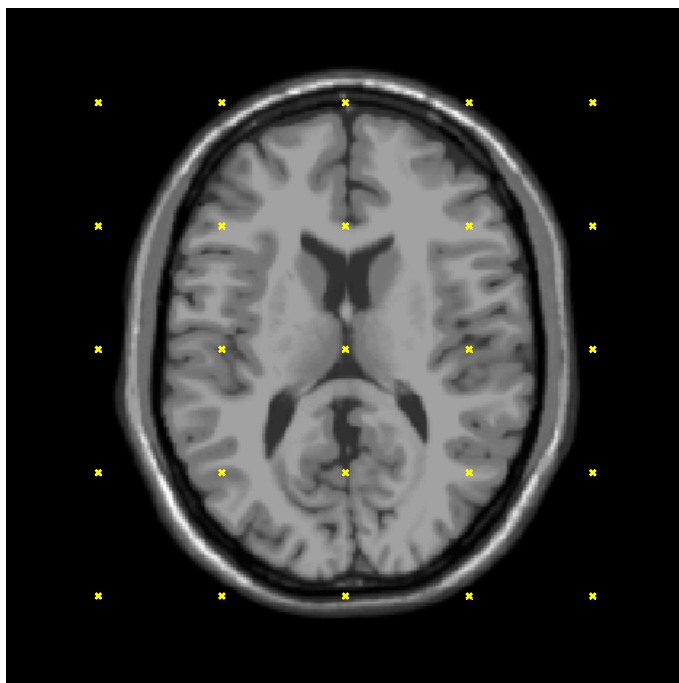


Fig. 3. Control points used for pair-wise registration. Control points are denoted as x. Twenty five control points are uniformly distributed.

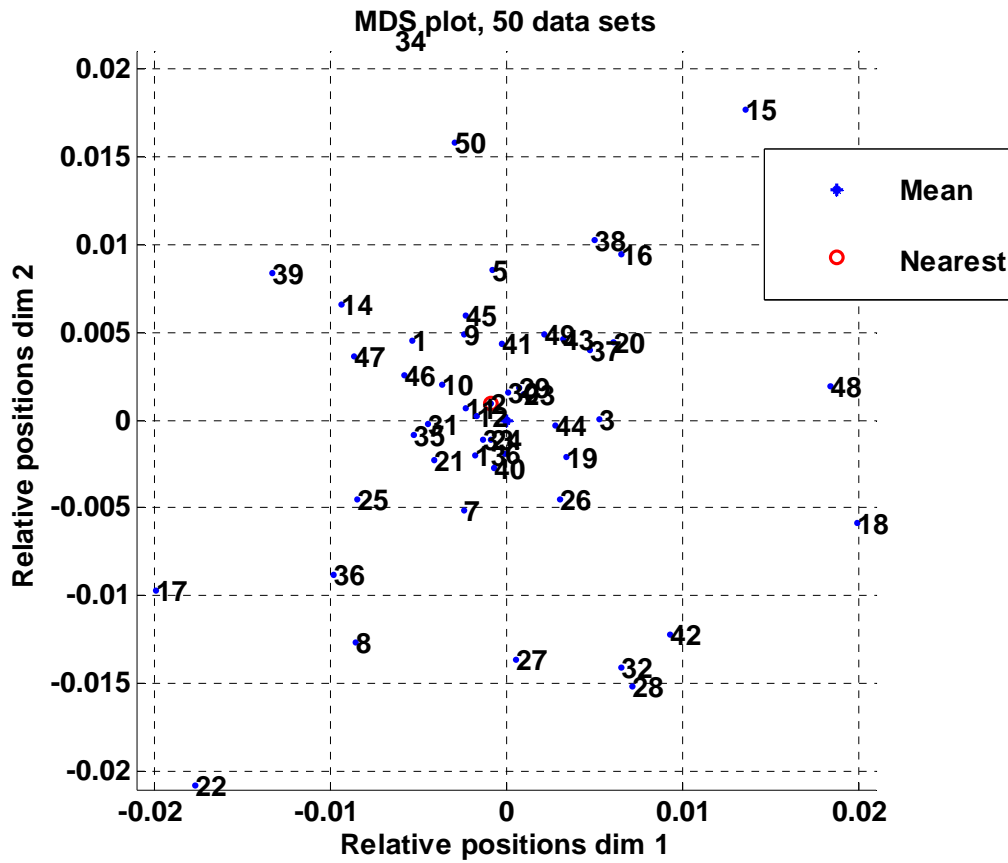


Fig. 4. Relative locations of 50 images by MDS. Mean location is at (0,0,0,0) and the closest image to mean is determined to be image 2. Only a 2 dimensional plot (out of 4) is given here for space constraints. Mean is marked with '+' and the nearest image to the mean is marked with 'o'.

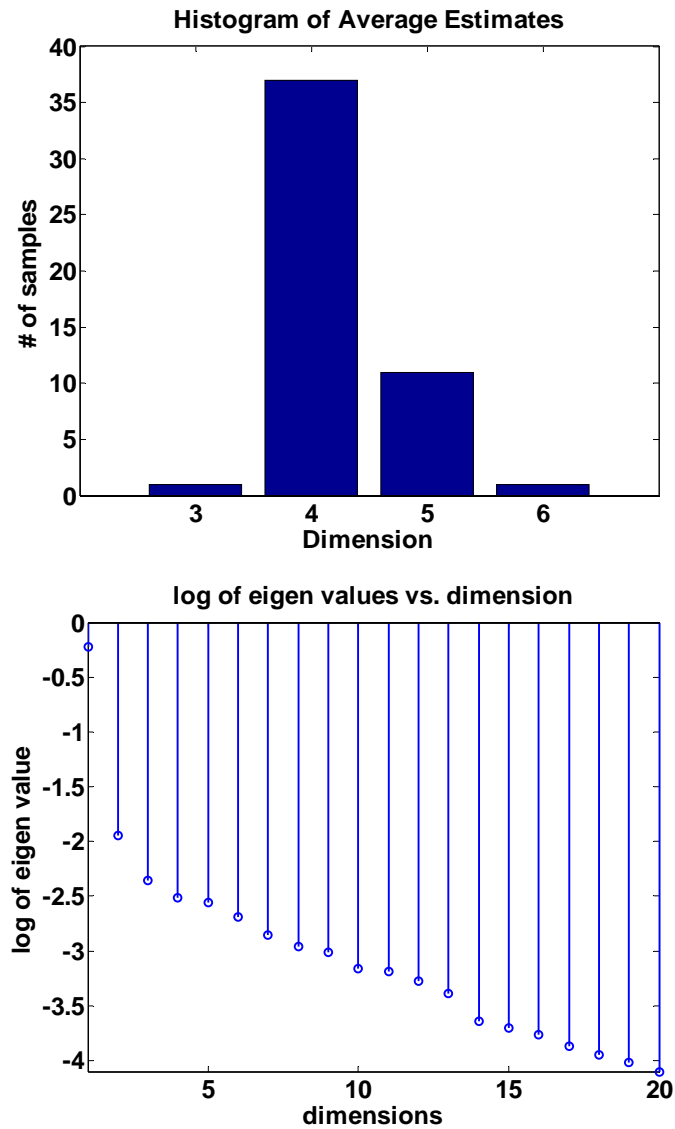


Fig. 5. Plot of dimension histogram of entropic graph estimator [20] and eigenvalues of the distance matrix. The top plot is the dimension histogram of entropic graph dimension estimator. Manifold learning is performed for the distance matrix as explained in section 3.3. The most probable dimension (mode) is dimension 4. The bottom plot is the logarithm of eigenvalues of the distance matrix with respect to the dimension of MDS. First 20 values out of 50 are plotted.

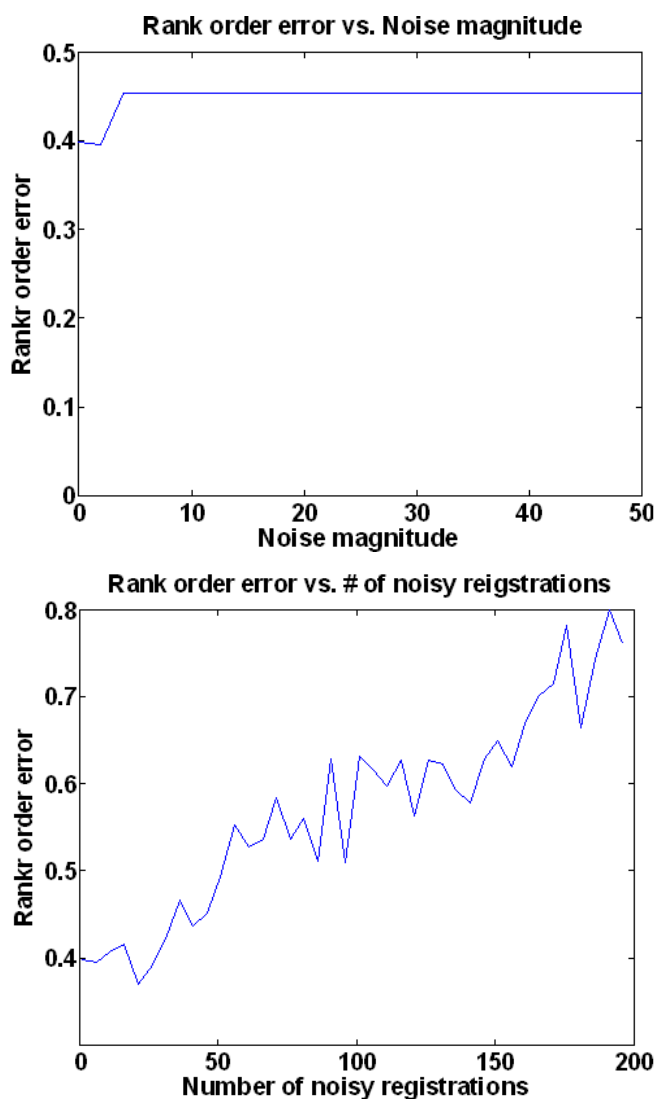


Fig. 6. Plot of rank order error with respect to noisy registrations. The top plot is the rank order error measured as the noise magnitude increases for one pair-wise registration. The affected pair-wise registration is between image 9 and 45. The bottom plot is the rank order error measured as the number of affected pair-wise registration increases. The magnitude of registration noise is set at zero mean Gaussian with standard deviation 15 pixels.

Table 1. Distances from the original undeformed image. Geometric distances are sorted ascendingly. Images with small distances are desirable as the target image. Image 2 is the most desirable target image and image 4 is the least desirable target image.

Distance	0.0009	0.0116	0.0269	0.0282	0.0286	0.0388	0.0413	0.0554	0.0652
Image No.	2	30	12	44	23	40	33	29	24
Distance	0.0693	0.0718	0.0729	0.0763	0.0836	0.0866	0.0875	0.1066	0.1088
Image No.	41	46	20	7	21	1	10	45	37
Distance	0.1194	0.1307	0.1361	0.1607	0.1657	0.1669	0.1956	0.1981	0.2016
Image No.	49	26	43	31	19	47	5	14	13
Distance	0.2219	0.2285	0.2303	0.2334	0.2476	0.3647	0.4034	0.4403	0.4503
Image No.	16	11	25	35	27	36	42	39	9
Distance	0.4706	0.4845	0.4871	0.5511	0.5527	0.5654	0.5811	0.6103	0.651
Image No.	15	48	8	6	28	34	18	3	50
Distance	0.6685	0.6944	1.0705	1.0835	1.3823				
Image No.	32	17	22	38	4				

Table 2. MDS results. Image number is sorted by the distance from the location of mean geometry. Distances are sorted ascendingly. The order of image number is very similar to the order of image number in Table 1. RMS (root mean squared) error between the order of image number by MDS and order of image number of the ground truth is computed on the bottom row.

Order	1	2	3	4	5	6	7	8	9
Image No.	2	30	23	40	44	12	29	24	21
Order	10	11	12	13	14	15	16	17	18
Image No.	33	41	10	46	7	1	26	37	49
Order	19	20	21	22	23	24	25	26	27
Image No.	20	31	45	19	43	47	13	14	35
Order	28	29	30	31	32	33	34	35	36
Image No.	5	11	27	16	25	42	39	36	9
Order	37	38	39	40	41	42	43	44	45
Image No.	28	3	18	8	34	48	32	6	15
Order	46	47	48	49	50				
Image No.	50	17	22	38	4				
Error	0.3980								